Research Square

Preprints are preliminary reports that have not undergone peer review.
They should not be considered conclusive, used to inform clinical practice,
or referenced by the media as validated information.

Cobalt-Based Drug Delivery to the Brain using Rapid Short-Pulses of Focused Ultrasound and Microbubbles reduces Aβ aggregation in 5XFAD mice

Sophie V. Morse

sophie.morse11@imperial.ac.uk

Imperial College London

Lucia Rohfleisch
Imperial College London

Grainne Geoghegan
Imperial College London

Krit Sujarittam
Chiang Mai University

Sarah Rimer
Imperial College London

Tiffany G. Chan
Imperial College London

Timothy Kench
Imperial College London

Maria Afonso Pereira
Imperial College London

Qiyixing Ethan Liu
Imperial College London

Bibiana Mota
Imperial College London

Robertas Aleksynas
Imperial College London

Laura Abelleira Hervas
Imperial College London

Varshini Packiyathasan
Imperial College London

Rishabh Sankar
Imperial College London

Zhi Ji
Imperial College London
Omer Faruk Dogru
Imperial College London
William Lim Kee Chang
Imperial College London
Ramon Vilar
Imperial College London
Magdalena Sastre
Imperial College London
James J. Choi
Imperial College London

Article

Keywords: focused ultrasound, microbubbles, blood-brain barrier, anti-aggregation cobalt-based drug, Alzheimer's disease, Amyloid-β

Posted Date: July 24th, 2026

DOI: https://doi.org/10.21203/rs.3.rs-10332117/v1

License: This work is licensed under a Creative Commons Attribution 4.0 International License.
Read Full License

Additional Declarations: No competing interests reported.

Abstract

A major obstacle to effective Alzheimer's disease therapy is the limited ability to deliver therapeutics across the blood-brain barrier. Focused ultrasound with microbubbles can transiently increase BBB permeability, and rapid short-pulse (RaSP) sequences have been shown to improve the safety and efficiency of this approach. Here, we investigated whether repeated RaSP-ultrasound treatments could deliver the cobalt-based compound CoLAm2, an inhibitor of amyloid-β (Aβ) oligomerization, to the brains of 5xFAD mice. Five-month-old mice received three weekly treatments consisting of intravenous CoLAm2 (5 mg/kg) and targeted BBB opening in the left hippocampus using RaSP ultrasound sequences. Immunohistochemistry demonstrated a 60.5% reduction in Aβ plaque area in mice receiving combined focused ultrasound and CoLAm2 compared with ultrasound-only, drug-only, and untreated controls. Ultrasound-only treatment also reduced aggregated Aβ by 35.6%, as assessed by Thioflavin S staining. Open field and novel object recognition tests detected no adverse effects on locomotor activity, anxiety-like behaviour, or cognition following repeated treatments. These findings demonstrate that repeated RaSP-ultrasound enables safe delivery of a small-molecule therapeutic across the BBB and enhances its anti-amyloid effects in a mouse model of Alzheimer's disease, supporting further investigation of this approach for neurological disorders.

1 Introduction

Alzheimer's Disease (AD) is the leading cause of dementia, accounting for approximately 60–70% of cases, with an estimated 57 million people living with dementia worldwide (WHO, 2023). This disease is characterized by progressive memory impairment alongside deficits in other cognitive domains, including executive function.[1–3]

One of the hallmark pathological features of AD is the formation of amyloid-β (Aβ) plaques, primarily located in the cerebral cortex and hippocampus.[4] Although the role of Aβ in AD has yet to be fully elucidated, there is evidence that it is involved in neuronal death and the inflammatory response observed in AD brains. In fact, current AD therapeutic approaches target Aβ deposition, including passive immunization.[5] However, more recent evidence suggests that it is not the Aβ plaques themselves that lead to neuronal loss and the aforementioned symptoms, but rather the Aβ oligomers (AβOs), which seem to possess the most neurotoxic properties. These AβOs build up in the early stages of the disease, preceding the formation of plaques. Therefore, targeting these aggregated states of Aβ is a valid treatment strategy.[6,7]

The N-terminal domain of Aβ monomers (residues 1–16), which aggregate to form AβOs and plaques, contains a high-affinity metal-binding site; this interaction predisposes Aβ monomers to aggregate and generate reactive oxygen species when binding to endogenous metal ions.[8,9] Therefore, metal complexes that selectively target this region of Aβ proteins hold therapeutic potential.[10–12] However, the potential of this approach has yet to be fully realized, with only a few examples of such metal complexes

having undergone *in vivo* testing, mainly due to concerns regarding their toxicity or their inability to cross the blood-brain barrier (BBB).[13–19]

To reach their targets in the brain in therapeutically relevant concentrations, these metal complexes must overcome the challenge of crossing the BBB. The BBB regulates homeostasis and prevents potentially harmful substances from entering the brain parenchyma, where the microenvironment is tightly controlled. However, this strict regulation prevents most small molecules < 400–500 Da and nearly all large molecules from crossing the BBB.[20]

The combination of focused ultrasound (FUS) and microbubbles is a promising method to enhance the permeability of the BBB in a non-invasive, targeted and transient manner.[21] This technique involves the intravenous administration of microbubbles and the desired therapeutic agents, combined with the application of a focused ultrasound beam to specific regions of interest in the brain. Upon entering the region of the cerebral vasculature that is exposed to the ultrasound beam, microbubbles oscillate radially, inducing mechanical stress on the surrounding vasculature which enhances the permeability of the BBB, temporarily allowing drugs into the brain. Numerous small molecules, DNA, antibodies, nanoparticles, and cells have been successfully delivered into the brain of rodents and non-human primates using this method, with ongoing human trials showing promising results.[22–31]

Conventional ultrasound sequences for this method of BBB enhancement consist of long pulses of ultrasound (pulse length > 10 ms) emitted at a slow rate (≤ 10 Hz).[25,32–39]. However, the use of short pulses of ultrasound emitted at a fast repetition rate and grouped into bursts has been shown to deliver compounds across the BBB efficiently and with an improved safety profile.[24,40–44] Short pulses enable more uniform drug delivery within the targeted region, with no or minimal red blood cell extravasation and rapid BBB permeability recovery within 10–20 minutes after ultrasound exposure, resulting in minimal disruption (center frequency = 1 MHz, peak-negative pressure = 0.35 MPa).[24]

We have previously shown that a cobalt-based compound (**CoLAm2** – see Supplementary Material for molecular structure), which targets the N-terminal domain of Aβ and inhibits its aggregation, can be delivered across the BBB using rapid short-pulses of focused ultrasound with microbubbles, with no changes in body weight or behavior after four weekly treatments in healthy wild-type and 5xFAD mice.[18] Here, we report the findings from a longitudinal study in which we aimed to investigate the therapeutic effect of repeated ultrasound-mediated delivery of a more water-soluble version of this cobalt-based compound to the left hippocampus of the brain, evaluating its efficacy in reducing aggregated Aβ in 5xFAD mice.

2 Materials and methods

2.1 Animals and study design

All procedures involving animals were conducted in accordance with the UK Animals (Scientific Procedures) Act 1986 and approved by Imperial College London's Animal Welfare and Ethical Review Body. 35 male 5xFAD mice (mean age = 4.91 ± 0.17 months) and 17 C57bl/6 wild-type mice (mean age = 4.89 ± 0.17 months) were used in this study (original strain obtained from Jax, strain B6SJL-Tg(APPSwFlLon,PSEN1*M146L*L286V)6799Vas/Mmjax, then bred and crossed with C57Bl6 mice from Charles River as heterozygous in-house). 5XFAD transgenic mice overexpress the human APP gene (APP695) with Swedish (K670N/ M671L), Florida (I716V) and London FAD mutations (V717I), as well as human Presenilin1 (PS1) with M146L and L286V FAD mutations (Oakley et al., 2006). They develop intraneuronal Aβ42 as early as 1.5 months, plaques and gliosis at 2 months, with cognitive deficits detectable at 4–5 months and neuronal loss starting at 6 months of age (Oakley et al., 2006, and own observations). A reversed 12:12 hour light/dark cycle was maintained for the animals, and food and water were provided ad libitum. Mice were acclimated for 7 days prior to starting the treatment regimen.

2.2 Ultrasound setup and experimental conditions

Mice were anaesthetized using a mixture of 1.5% – 2.0% vaporized isoflurane (Zoetis UK Limited, London, UK) delivered with oxygen at a flow rate of 1 L/min through an anesthetic vaporizer (Harvard Apparatus, Cambridge, UK). The fur on the head was removed with an electric trimmer followed by the application of depilatory cream, and the head was secured in a stereotaxic frame equipped with 45° ear bars (World Precision Instruments, Hertfordshire, UK).

Ultrasound gel was then applied to the mouse's head, and a water bath with a transparent parafilm membrane base was filled with degassed water and pressed against the gel and the top of the head. This setup facilitated visualization of the skull sutures for targeting. A 1-mm-thick metal cross was placed at the bottom of the water bath in alignment with the lambdoid and sagittal sutures as a reference point for positioning the transducer above the targeted region of the brain.[22]

The left hippocampus was chosen as the target region, with the ultrasound beam positioned 3 mm lateral to the sagittal suture, 0.5 mm anterior to the lambdoid suture, and 3 mm below the skull surface.[24] This region was chosen due to the lower attenuation of the parietal bone and the significance of the hippocampus as a potential therapeutic target, being a key memory center affected in Alzheimer's disease.

The transducer was operated in pulse-echo-mode, linked to a pulser-receiver (DPR300; Insidix, Seyssins, France) and moved using a computerized 3D positioning system (Velmex Inc., Bloomfield, NY, USA). Once the target was located, a single-element spherical-segment focused ultrasound was used to emit the therapeutic ultrasound pulses. The focal region of the 1-MHz transducer (Sonic Concepts, H-198; focal depth 60.5 mm, diameter: 90mm) had dimensions of 1 mm (elevational), 1.35 mm (lateral), and 20 mm (axial), as defined by the full-width at half-maximum of the acoustic pressure field. These pulses were generated using two function generators (33500B Series; Agilent Technologies, Santa Clara, CA, USA), amplified by a 50-dB power amplifier (Precision Acoustics Ltd., Dorchester, UK), and transmitted through the transducer. The mouse brains were exposed to ultrasound in a RaSP sequence, comprising

of thirteen 5-cycle pulses emitted at a pulse repetition frequency of 1.25 kHz and grouped into 10 ms bursts and emitted at a burst repetition frequency of 0.5 Hz.

Acoustic emissions from the microbubbles within the cerebral vasculature were captured during the ultrasound treatments using passive acoustic mapping (PAM) with a L7-4 linear array (number of elements: 128, aperture size: 38.1 mm, element spacing: 0.298 mm) placed through the rectangular cutout of the single-element 1 MHz therapeutic ultrasound transducer. The linear array was connected to an ultrasound imaging engine (Vantage, Verasonics, Kirkland, WA, USA) controlled by a PC. This detector was coaxially aligned through the rectangular central opening of the therapeutic transducer.

2.2.1 Cobalt-based drug administration

The cobalt complex (**CoLAm2;** concentration: 5 mg/kg; see Fig. S1) was prepared and isolated following slight modifications of the procedure reported previously.[18] This complex was injected intravenously over 30 s through a 30 G catheter before the ultrasound treatment. Ten seconds into the ultrasound – allowing five control pulses to be emitted – *SonoVue*® microbubbles (Bracco, Milan, Italy) were subsequently injected through the same catheter over a 30 s period (concentration: 5 µL/g body mass, vial concentration: 3×10^8/mL). Microbubbles were activated following manufacturer instructions and used within 6 h from activation.

The above procedure was performed once a week for a total of three weeks (Fig. 1). In all treated mice, the RaSP sequence of focused ultrasound was applied to the left hippocampus, leaving the right hippocampus, which was not exposed to ultrasound, as a control. Treatment groups included the following: healthy wild-type untreated mice and then 5xFAD Alzheimer's mice with either no treatment, drug only, focused ultrasound + vehicle injection (FUS + Vehicle), or focused ultrasound + drug (FUS + drug).

2.3 Acoustic emissions quantification

The degree of microbubble activity was estimated to explore whether it correlated with plaque reduction. The bubble emissions received by the L7-4 linear array were quantified using the axial-temporal positioning beamforming algorithm previously described by Davies et al. (2021)[40], yielding an acoustic energy map (coronal imaging plane, 5 µs signal window length, 0.1-by-0.1-mm pixel size, 1486 m/s nominal speed of sound). For each sonication session, all acoustic energy maps obtained during the treatment pulses were added together, forming an accumulated acoustic energy map. The means and variances of the acoustic energy near the foci were then calculated. For each map, the center of bubble activity was located. The map was binarized, highlighting the area where active bubbles are present and the centroid of this shape was determined as the center. A 2-by-5 mm region of interest around the centroid was then defined, with the long side running parallel to the direction of wave propagation. The dimensions were chosen such that the lateral dimension was slightly larger than the 6-dB lateral size of the ultrasonic beam, and the axial dimension was approximately equal to the depth of the brain. Only the

pixels whose values were greater than two standard deviations above the average value were deemed to contain signals from microbubbles and were carried forward for further processing. The mean and variance of these pixel values were calculated, with the mean and variance values being indicative of the average degree of microbubble activity inside the brain and the spread of these activities respectively within each mouse.

A potential correlation between the energy of the recorded microbubble activity and plaque reduction was explored. Plaque quantities (vertical axes) were plotted against the sum of the mean acoustic energy from across the three ultrasound treatments for each mouse (horizontal axes). The horizontal error bars indicate the square root of the combined variances.

2.4 Behavioral testing

To examine the behavioral effects of the treatment regimen, open field testing and novel object recognition testing were carried out as previously reported. Open field testing was used to assess changes in locomotor functions, anxiety levels and overall exploratory behavior, while novel object recognition was used to identify impairments in recognition memory. Open field testing was conducted 72 hours after the last ultrasound treatment with novel object recognition training being performed immediately after, with novel object recognition testing was performed 24 hours after that. The full protocol is described in the Supplementary Information.

2.5 Tissue processing and immunofluorescence staining

After completion of the behavioral tests, the mice were euthanized with pentobarbital sodium overdose and transcardial perfusion using 20 mL of ice-cold PBS containing (20 units/mL), followed by 20 mL of 10% formalin (Sigma Aldrich, St Louis, MO, USA), 5 days after the last ultrasound treatment. The brain was then extracted and half the brain (anterior) was snap-frozen for subsequent analysis with Westerns and ELISAs, while the other half (posterior including the hippocampus) was fixed in 10% formalin overnight, followed by a transfer into 30% sucrose for cryoprotection overnight and sectioning into 30-µm-thick horizontal slices using a cryostat (CryoStar NX70; Thermo Fisher, Waltham, MA, USA). The sections spanned the entire hippocampus, with the cryostat's specimen head temperature set to -14°C and the blade temperature to -12°C.

2.5.1 Thioflavin-S staining

To determine changes in Aβ aggregation, brain sections were incubated in Thioflavin-S (Thio-S, Sigma-Aldrich) solution (1% (w/v) Thio-S in 70% ethanol) at room temperature for 10 minutes. Following this, sections were washed with 70% ethanol (3x 5 min) and then with PBS (1x 5 min), and then mounted on slides with Prolong Gold antifade (Invitrogen).

2.5.2 MOAB-2 fluorescence staining for Aβ load

Brain sections were initially washed in Tris-buffered saline (TBS; 3x 5 min), then permeabilized using 0.25% Triton X-100 (Tx) in TBS for 30 minutes. The sections were then washed again in TBS (3x 5 min)

and blocked for 60 minutes in a solution containing 5% donkey serum and 1% bovine serum albumin (BSA) in 0.1% Tx-TBS. Subsequently, sections were incubated overnight at 4°C with a primary mouse anti-amyloid-β MOAB-2 antibody (1:200, ab126649, Abcam) in 0.01% Tx-TBS containing 0.1% BSA. The next day, sections were washed in TBS (3x 5 min) and incubated with a secondary fluorescent donkey anti-rabbit IgG H%L (Alexa Fluor 488) antibody (1:500, ab150073, Abcam) for 120 minutes at room temperature. Sections were then washed in TBS (4x 5 min), followed by a 5-minute wash in PBS. To reduce anti-fluorescence, sections were incubated in 0.1% Sudan Black in 70% ethanol for 20 minutes and then washed under distilled running water for 10 minutes. Finally, a DAPI (4,6-diamidino-2-phenylindole) counterstain (ab104139, Abcam) was applied for 5 minutes for visualize cell nuclei.

2.5.3 Microglial fluorescence staining

An ionized calcium-binding adaptor molecule 1 (Iba1) antibody was used as a marker of microglia. Sections were washed and incubated in a permeabilization and then blocking solution as per standard protocol (washing: 3x 5 min in TBS before and after permeabilization; permeabilization: 0.25% Tx in PBS for 30 min; blocking: 5% donkey serum + 1% BSA in TBS + 0.1% Tx for 60 minutes). After incubation overnight at 4°C with a primary goat anti-Iba1-antibody (ab5076; Abcam), the sections were washed again in TBS (3x 5 min). Subsequently, secondary antibody incubation was performed with a rabbit fluorescent anti-goat IgG H&L Alexa Fluor 647 for 2 hours (ab150143; Abcam) at room temperature. Following the incubation, the sections were washed (4x 5 min in TBS and 1x 5 min in PBS) and counterstained for 5 min with DAPI to visualize cell nuclei, following Sudan Black (0.1% Sudan black in 70% ethanol) for 20 minutes and washing with distilled water (10 min).

2.5.4 Imaging and Quantification

Images of brain sections stained for Thio-S, MOAB-2 and Iba1 were obtained by fluorescence microscopy (10x; Zeiss Axio Observer; Oberkochen, Germany). Thio-S or MOAB-2-stained slices were excited at 470/40 nm and emissions filtered at 525/50 nm, while Iba-1-stained slices were excited at 640/30 nm and emissions filtered at 690/50 nm. The number, mean area, and percentage of area covered by protein aggregates (Thio-S) and amyloid-β (MOAB-2) was quantified from the images within a selected region of interest incorporating both the hippocampus and adjacent thalamus region using Fiji ImageJ v.2.14.0 (Fiji, Bethesda, MD, USA). If present, artefacts, such as folds and air bubbles, were avoided. The number of microglia co-localizing with protein aggregates was quantified by three blinded counters and averaged.

2.6 Statistical analysis

Statistical analyses were performed using GraphPad Prism 8 software (GraphPad Software Inc, Boston, MA, USA). To confirm whether the data was normally distributed, we ran Kolmogorov-Smirnov tests. Levene's test was performed to confirm homogeneity of variances. Data were analyzed with unpaired Student's t-tests, simple linear regression, and repeated-measures one-way analyses of variance (ANOVA), followed by Tukey's *post hoc* analysis. A probability of less than 0.05 was considered significant. All quantitative data are given as mean ± SD.

3 Results

In vivo delivery of cobalt-based drug with focused ultrasound results in reduced Aβ aggregates

In a previous *in vitro* study, we showed that this **CoLAm2** cobalt-based drug prevented the aggregation of monomeric Aβ into oligomers and therefore Aβ aggregates.[18] Here, to assess its efficacy *in vivo* following ultrasound-mediated delivery, we stained brain sections for protein aggregates as well as all forms of Aβ, including monomers, oligomers and plaques, while also co-staining for Iba1 + microglia surrounding the protein aggregates.

Staining with Thio-S revealed a significant 59.2% reduction in the number of Aβ plaques and a 60.5% decrease in the percentage area covered by Aβ protein aggregates decreased significantly in the left hippocampus and thalamus of 5xFAD mice in the FUS + Drug group compared to the no treatment group (Fig. 2a-f), suggesting a reduction in aggregated Aβ following the delivery of this drug. Interestingly, we also observed a reduction in Thio-S staining in the FUS-only group by 32.2% (number of Aβ plaques) and 35.6% (percentage of area covered by Aβ plaques) compared with untreated controls. No difference was detected in the mean plaque area between treatment groups ($P > 0.05$, Fig. 2g), indicating that the treatments did not affect the size of the protein aggregates.

Following this, we examined whether the reduction in Thio-S staining reflected a decrease in total Aβ load. We, therefore, stained for Aβ monomers, oligomers, and aggregates using the MOAB-2 antibody, rather than just aggregates as detected by Thio-S. Analysis of the percentage of area covered, the number of Aβ plaques detected, and mean area of Aβ expression in the hippocampus showed no significant differences between treatment groups (Fig. 3a-g).

To assess any possible effects outside of the ultrasound-targeted region, extracts from the frontal cortex obtained by subcellular fractionation were assessed for changes in the levels of monomers (Aβ1–40 and Aβ1–42) and aggregates by performing western blots and ELISAs. No significant differences were observed in the amount of Aβ proteins detected with western blots (Figure S1). Additionally, no differences were observed in the concentration of Aβ subtypes in the soluble and detergent-soluble fractions by ELISA (Figure S2).

During the ultrasound treatments, monitoring was performed by measuring the acoustic emissions from the microbubbles using passive acoustic mapping (PAM). The acoustic energy from these emissions was measured and correlated with the average number of plaques detected in FUS + Vehicle and FUS + Drug treatment groups. The number of plaques decreased with increasing acoustic energy from the microbubble emissions in the FUS + Drug treated mice, suggesting these emissions could be used to guide treatment monitoring ($R^2 = 0.89$; Fig. 4b). However, the average number of plaques increased with increasing acoustic energy ($R^2 = 0.68$) in FUS + Vehicle treated mice (Fig. 4a), which warrants further investigation.

Delivery of cobalt-based CoLAm2 drug using rapid short-pulses of focused ultrasound results in less microglia surrounding Aβ plaques

Microglia play an important role in clearing unwanted compounds from the brain via phagocytic functions[46] and in AD brains they appear surrounding Aβ plaques.[5] By staining for Iba1 + microglia, we intended to determine whether microglia were involved in the clearing of protein aggregates observed following ultrasound treatments.

Co-staining for Iba1 + microglial cells and Thio-S protein aggregates showed a reduction in the number of microglia co-localizing with protein aggregates in mice treated with FUS + Drug in comparison with other treatment groups (Fig. 5a-l). Quantification showed the reduction to be greatest between the FUS + Drug and no treatment groups (33.0% reduction; $P < 0.0001$), and also significant compared with FUS + Vehicle mice (12.9% reduction; $P < 0.05$; Fig. 5m).

Cobalt-based CoLAm2 drug delivered across the blood-brain barrier with focused ultrasound does not affect cognitive or motor behavior

Behavioral testing was performed with both open field tests, as a measure of anxiety, activity and locomotion, as well as novel object recognition tests, to measure recognition memory. No significant differences were observed in open field tests ($P > 0.05$; Fig. 6a-g) in the behavior of 5xFAD mice of all treatment groups and healthy wild-type (WT) mice in terms of anxiety (Fig. 6a-c), activity (Fig. 6d-e) and locomotion (Fig. 6f-g) measurements. Novel object recognition tests showed no effects of any of the treatments on cognition ($P < 0.05$; Fig. 6 (**h-i**)). No differences were detected in the discrimination index between treatment groups ($P > 0.05$; Fig. 6 (**j**)). These results highlight that none of the treatments affected these types of behavior in a negative way, in particular, 5xFAD showed no differences in comparison with healthy wild-type mice at this age.

4 Discussion

This study is the first to show that a therapeutic effect can be achieved by emitting Rapid Short-Pulses of focused ultrasound in a chronic treatment regimen *in vivo* in a model of Alzheimer's disease. We successfully delivered a novel cobalt-based drug, **CoLAm2**, which could safely and effectively prevent further progression of AD pathophysiology. Our results support the hypothesis that **CoLAm2** primarily prevents the formation of new oligomers rather than affecting pre-existing plaques, since the mean plaque area (which reflects the size of the plaques) was similar between treatment groups. Since treatments began at four to five months of age, the 5xFAD mice would have already developed protein aggregates. However, future work would need to validate whether this is the case.

Previously, we have shown that this cobalt complex was able to prevent the aggregation of Aβ monomers into oligomers *in vitro*, and therefore we hypothesized that this would result in a reduction in Aβ plaques in vivo. These results provide the first evidence that this drug can effectively reduce the formation of plaques over time *in vivo*.

Because this compound does not cross the BBB, we used focused ultrasound in combination with microbubbles to deliver this drug. Specifically, we employed Rapid Short-Pulse (RaSP) sequences of focused ultrasound, which lead to uniform drug distributions within the targeted brain area while maintaining a high safety profile.[24,42]

The differences observed in both the number of plaques and the percentage of area covered by protein aggregates, as detected by Thio-S, support the effectiveness of the drug delivery procedure and the compound itself. Interestingly, a reduction in plaque count as well as in plaque area covered was observed when using FUS in combination with microbubbles without the drug (only injecting a vehicle solution), albeit to a lesser extent than in the condition with the delivered compound. This is in line with findings from other studies which show a reduction in Aβ with ultrasound-mediated BBB permeability increase.[47–49] It is hypothesized that this effect may be due to the entry of bloodborne substances into the brain, triggering clearance mechanisms such as the activation of microglia and astrocytes.

The lack of significant differences detected in all forms of Aβ between ultrasound-treated mice and the control groups could indicate a lower presence of oligomers and aggregates with a higher presence of monomers, as expected with this drug. The slight trend in decrease in the mean Aβ area detected with MOAB-2 staining could indicate a higher presence of smaller areas of fluorescence (monomers) compared to larger ones (oligomers and aggregates).

To assess potential off-target effects of the treatment we performed ELISAs and western blots on cortex samples, known to be more sensitive than staining.[50,51] The lack of differences observed in the number of aggregates detected via western blotting and the number of monomers detected with ELISAs, implies that no off-target effects could be detected in the cortex 5 days after ultrasound treatments, following the behavioral testing performed in this study. Future work would need to determine whether changes can be detected at earlier timepoints.

Unlike approaches that reduce Aβ production, aggregation inhibitors, like **CoLAm2**, do not interfere with the normal physiological processing of APP or other substrates, potentially avoiding mechanism-related off-target effects.[10,11] Secretase inhibitors, which reduce Aβ production upstream, have largely failed in clinical trials due to mechanism-related toxicity arising from the inhibition of essential physiological substrates such as Notch, leading to cognitive worsening and other adverse effects in patients.[52,53] Anti-Aβ monoclonal antibodies, while achieving clinical approval and demonstrating robust amyloid clearance, are associated with amyloid-related imaging abnormalities (ARIA) including cerebral edema and microhemorrhages, and their cognitive benefits have been modest and remain debated.[54,55] Small-molecule aggregation inhibitors such as **CoLAm2** may therefore offer a complementary approach that circumvents both the mechanism-related toxicities of secretase inhibition and the immune-mediated side effects associated with immunotherapies.

Previous studies have shown an increase in microglial presence around Aβ plaques following ultrasound treatments,[56] suggesting that ultrasound combined with microbubbles alone can enhance microglial-

mediated Aβ clearance.[48] However, these studies were performed using long pulses of ultrasound, which could affect microglia differently compared to RaSP treatments. In our study using rapid short-pulse sequences, the ratio of microglia co-localizing with protein aggregates (detected with Thio-S) in comparison with the total number of Iba1 + microglia was reduced in mice treated with FUS + Drug. This result could be explained by the reduction in protein aggregates due to the presence of **CoLAm2**, leading to a reduction in the phagocytic response from these microglial cells.[57] Previous work has shown that RaSP sequences lead to lower levels of blood-derived proteins entering the brain, which could also lead to lower degrees of activation in microglial phagocytic functions.[24,42] The use of RaSP sequences in contrast to long pulse ultrasound could therefore be the reason for the observed results. However, the significant difference between mice treated with FUS + Vehicle and those with FUS + Drug indicates an additional effect of the **CoLAm2** drug. This data was acquired at a single timepoint, 5 days after the last ultrasound treatment; it would therefore be interesting to look at how microglial presence varies around the plaques at earlier timepoints.

Behavioral results showed that none of the treatments affected anxiety, activity, locomotion or recognition memory. These results confirm that three weekly treatments with RaSP ultrasound sequences with or without the **CoLAm2** cobalt-based drug being delivered, do not have a negative impact on the behavior of these mice in comparison with that of healthy wild-type mice. Future work intending to assess whether longitudinal treatments could improve cognitive functions should employ mice at an age that display behavioral deficits. Also, in this study ultrasound was only focused onto the left hippocampus, using the right hippocampus as an internal control, therefore behavioral improvements were not expected. Future work should consider targeting both hippocampi and/or other brain networks associated with AD symptomatology, as well as using other behavioral tests to analyze hippocampal-mediated memory, such as the Y maze, object location test or fear conditioning.

As shown in previous work,[58–60] higher levels of microbubble activity during ultrasound-mediated drug delivery generally correlate with better treatment outcomes, such as the lower number of plaques detected in FUS + Drug treated mice in this study. When ultrasound was used to increase the permeability of the blood-brain barrier without a drug, however, higher microbubble activity did not correlate with a reduction in the detected plaques in this study.

To be able to extrapolate these results to human studies, future investigations should evaluate the effects of these treatments in other animal models as well as older animals to provide further understanding. Given that AD pathology involves widespread neural networks, including cortical and subcortical regions, future studies will explore the impact of targeting broader areas or multiple brain regions simultaneously. Such an approach may yield more pronounced behavioral improvements and offer a clearer understanding of the therapeutic implications of RaSP ultrasound treatments. Future studies will also aim to determine how effects might vary across different age groups to capture variability in disease progression and therapeutic responses.

This chronic ultrasound regimen was evaluated over a relatively short period, with outcomes measured five days after the final treatment. Consequently, shorter and longer-term effects of these interventions remain unclear. Extended longitudinal studies with longer follow-up periods will be essential to determine the durability of these effects and their potential to translate into meaningful clinical benefits.

In conclusion, this study marks both the first proof-of-concept of a safe chronic RaSP FUS treatment as well as the efficacy of the **CoLAm2** cobalt-based compound for Alzheimer's disease *in vivo*. Administered once a week for three weeks, this approach successfully delivered this compound to the targeted brain region and achieved a reduction in protein aggregates. By demonstrating the feasibility and effectiveness of this treatment approach, this study provides a foundation for further exploration of RaSP focused ultrasound as a non-invasive and versatile technique for the treatment of a wide spectrum of neurological and neuropsychiatric diseases. Continued exploration of this innovative approach may ultimately pave the way for meaningful clinical applications.

Declarations

Author Contributions Statement

S.V.M. conceived the study, designed and performed the experiments, analysed the data, prepared figures, wrote the manuscript, and acquired funding. L.R. acquired and analysed data, performed statistical analysis, prepared figures, and wrote and edited the manuscript. G.G. analysed data and edited the manuscript. K.S. analysed data, prepared figures, and wrote parts of the paper. S.R. prepared figures and contributed to writing the manuscript. T.G.C. contributed to the original conception of the study, performed experiments, and provided tissue analysis protocols. T.K. synthesised the drug used in the study and wrote the chemistry sections. B.M. performed in vivo experiments and assisted with behavioural testing. R.A. and L.A.H. helped with the performance and analysis of the ELISA and Western blot data. M.A.P., Q.E.L., V.P., R.S., Z.J., O.F.D. and W.L.K.C. analysed behavioural or staining data. R.V., M.S. and J.J.C supervised the study, acquired funding, and wrote and edited the manuscript. All authors reviewed the manuscript.

Author Contribution

S.V.M. conceived the study, designed and performed the experiments, analysed the data, prepared figures, wrote the manuscript, and acquired funding. L.R. acquired and analysed data, performed statistical analysis, prepared figures, and wrote and edited the manuscript. G.G. analysed data and edited the manuscript. K.S. analysed data, prepared figures, and wrote parts of the paper. S.R. prepared figures and contributed to writing the manuscript. T.G.C. contributed to the original conception of the study, performed experiments, and provided tissue analysis protocols. T.K. synthesised the drug used in the study and wrote the chemistry sections. B.M. performed in vivo experiments and assisted with behavioural testing. R.A. and L.A.H. helped with the performance and analysis of the ELISA and Western

blot data. M.A.P., Q.E.L., V.P., R.S., Z.J., O.F.D. and W.L.K.C. analysed behavioural or staining data. R.V., M.S. and J.J.C supervised the study, acquired funding, and wrote and edited the manuscript. All authors reviewed the manuscript.

Acknowledgement

Sophie V. Morse acknowledges funding for her Imperial College Research Fellowship and Engineering and Physical Sciences Research Council (EPSRC) doctoral prize fellowship. This work was also supported by the Alzheimer's Research UK charity (ARUK-IRG2017 A-7) to JJC and MS. Grainne Geoghegan is supported by an Imperial College London President's Scholarship, Tiffany G. Chan would like to acknowledge funding from the EPSRC Centre for Doctoral Training in Neurotechnology (EP/L016737/1). William Lim Kee Chang would like to acknowledge funding from the EPSRC Centre for Doctoral Training in Smart Medical Imaging (EP/S022104/1) and the Department of Bioengineering, Imperial College London. The authors would like to thank Meng-Xing Tang and Matthieu Toulemonde for generously providing access to and technical assistance with the Verasonics machine, and David Gaboriau for his imaging expertise. The Facility for Imaging by Light Microscopy (FILM) at Imperial College London is part-supported by funding from the Wellcome Trust (grant 104931/Z/14/Z) and BBSRC (grant BB/L015129/1). Figures were created with BioRender.com.

Data Availability

All data supporting the findings of this study are available within the paper and its Supplementary Information, or can be provided upon request from the corresponding author.

References

1. McKhann, G. et al. Clinical diagnosis of Alzheimer's disease: Report of the NINCDS-ADRDA Work Group* under the auspices of Department of Health and Human Services Task Force on Alzheimer's Disease. *Neurology* **34**, 939–939 (1984).
2. Kirova, A. M., Bays, R. B. & Lagalwar, S. Working Memory and Executive Function Decline across Normal Aging, Mild Cognitive Impairment, and Alzheimer's Disease. *BioMed Res. Int.* 1–9 (2015). (2015).
3. Guarino, A. et al. Executive Functions in Alzheimer Disease: A Systematic Review. *Front. Aging Neurosci.* **10**, 437 (2019).
4. Thal, D. R., Rüb, U., Orantes, M. & Braak, H. Phases of Aβ-deposition in the human brain and its relevance for the development of AD. *Neurology* **58**, 1791–1800 (2002).
5. Heneka, M. T., Morgan, D. & Jessen, F. Passive anti-amyloid β immunotherapy in Alzheimer's disease —opportunities and challenges. *Lancet* **404**, 2198–2208 (2024).

6. Shankar, G. M. et al. Amyloid-β protein dimers isolated directly from Alzheimer's brains impair synaptic plasticity and memory. *Nat. Med.* **14**, 837–842 (2008).
7. Figueiredo, C. P. et al. Memantine Rescues Transient Cognitive Impairment Caused by High-Molecular-Weight A Oligomers But Not the Persistent Impairment Induced by Low-Molecular-Weight Oligomers. *J. Neurosci.* **33**, 9626–9634 (2013).
8. Hane, F., Tran, G., Attwood, S. J. & Leonenko, Z. Cu2 + Affects Amyloid-β (1–42) Aggregation by Increasing Peptide-Peptide Binding Forces. *PLoS ONE*. **8**, e59005 (2013).
9. Marino, T., Russo, N., Toscano, M. & Pavelka, M. On the metal ion (Zn2+, Cu2+) coordination with beta-amyloid peptide: DFT computational study. *Interdiscip Sci. Comput. Life Sci.* **2**, 57–69 (2010).
10. Hayne, D. J., Lim, S. & Donnelly, P. S. Metal complexes designed to bind to amyloid-β for the diagnosis and treatment of Alzheimer's disease. *Chem. Soc. Rev.* **43**, 6701–6715 (2014).
11. Liu, H., Qu, Y. & Wang, X. Amyloid β-Targeted Metal Complexes for Potential Applications in Alzheimer's Disease. *Future Med. Chem.* **10**, 679–701 (2018).
12. Gomes, L. M. F., Bataglioli, J. C. & Storr, T. Metal complexes that bind to the amyloid-β peptide of relevance to Alzheimer's disease. *Coord. Chem. Rev.* **412**, 213255 (2020).
13. Heffern, M. C. et al. Modulation of Amyloid-β Aggregation by Histidine-Coordinating Cobalt(III) Schiff Base Complexes. *ChemBioChem* 15, 1584–1589 (2014).
14. Iscen, A. et al. Inhibition of Amyloid-β Aggregation by Cobalt(III) Schiff Base Complexes: A Computational and Experimental Approach. *J. Am. Chem. Soc.* **141**, 16685–16695 (2019).
15. Yellol, G. S. et al. Synthesis of 2-Pyridyl-benzimidazole Iridium(III), Ruthenium(II), and Platinum(II) Complexes. Study of the Activity as Inhibitors of Amyloid-β Aggregation and Neurotoxicity Evaluation. *Inorg. Chem.* **54**, 470–475 (2015).
16. Roberts, K. F. et al. Cobalt(III) Schiff base complexes stabilize non-fibrillar amyloid-β aggregates with reduced toxicity. *J. Inorg. Biochem.* **213**, 111265 (2020).
17. Heffern, M. C. et al. Tuning Cobalt(III) Schiff Base Complexes as Activated Protein Inhibitors. *Inorg. Chem.* **54**, 9066–9074 (2015).
18. Chan, T. G. et al. Modulation of amyloid-β aggregation by metal complexes with a dual binding mode and their delivery across the blood–brain barrier using focused ultrasound. *Chem. Sci.* **12**, 9485–9493 (2021).
19. Saini, R. et al. Inhibition of amyloid β1–42 peptide aggregation by newly designed cyclometallated palladium complexes. *Int. J. Biol. Macromol.* **248**, 125847 (2023).
20. Pardridge, W. M. The blood-brain barrier: Bottleneck in brain drug development. *NeuroRX* **2**, 3–14 (2005).
21. Hynynen, K., McDannold, N., Vykhodtseva, N. & Jolesz, F. A. Noninvasive MR Imaging–guided Focal Opening of the Blood-Brain Barrier in Rabbits. *Radiology* **220**, 640–646 (2001).
22. Choi, J. J., Pernot, M., Small, S. A. & Konofagou, E. E. Noninvasive, transcranial and localized opening of the blood-brain barrier using focused ultrasound in mice. *Ultrasound Med. Biol.* **33**, 95–104

(2007).

23. Park, J., Zhang, Y., Vykhodtseva, N., Jolesz, F. A. & McDannold, N. J. The kinetics of blood brain barrier permeability and targeted doxorubicin delivery into brain induced by focused ultrasound. *J. Controlled Release*. **162**, 134–142 (2012).
24. Morse, S. V. et al. Rapid Short-pulse Ultrasound Delivers Drugs Uniformly across the Murine Blood-Brain Barrier with Negligible Disruption. *Radiology* **291**, 459–466 (2019).
25. Chan, T. G., Morse, S. V., Copping, M. J., Choi, J. J. & Vilar, R. Targeted Delivery of DNA-Au Nanoparticles across the Blood–Brain Barrier Using Focused Ultrasound. *ChemMedChem* 13, 1311–1314 (2018).
26. Abrahao, A. et al. First-in-human trial of blood–brain barrier opening in amyotrophic lateral sclerosis using MR-guided focused ultrasound. *Nat. Commun.* **10**, 4373 (2019).
27. Lipsman, N. et al. Blood–brain barrier opening in Alzheimer's disease using MR-guided focused ultrasound. *Nat. Commun.* **9**, 2336 (2018).
28. Rezai, A. R. et al. Focused ultrasound–mediated blood-brain barrier opening in Alzheimer's disease: long-term safety, imaging, and cognitive outcomes. *J. Neurosurg.* **139**, 275–283 (2023).
29. Mehta, R. I. et al. Ultrasound-mediated blood–brain barrier opening uncovers an intracerebral perivenous fluid network in persons with Alzheimer's disease. *Fluids Barriers CNS*. **20**, 46 (2023).
30. Rezai, A. R. et al. Ultrasound Blood–Brain Barrier Opening and Aducanumab in Alzheimer's Disease. *N Engl. J. Med.* **390**, 55–62 (2024).
31. Bae, S. et al. Transcranial blood-brain barrier opening in Alzheimer's disease patients using a portable focused ultrasound system with real-time 2-D cavitation mapping. *Theranostics* **14**, 4519–4535 (2024).
32. Choi, J. J., Selert, K., Vlachos, F., Wong, A. & Konofagou, E. E. Noninvasive and localized neuronal delivery using short ultrasonic pulses and microbubbles. *Proc. Natl. Acad. Sci.* 108, 16539–16544 (2011).
33. Hynynen, K., McDannold, N., Sheikov, N. A., Jolesz, F. A. & Vykhodtseva, N. Local and reversible blood–brain barrier disruption by noninvasive focused ultrasound at frequencies suitable for trans-skull sonications. *NeuroImage* 24, 12–20 (2005).
34. McDannold, N., Arvanitis, C. D., Vykhodtseva, N. & Livingstone, M. S. Temporary Disruption of the Blood–Brain Barrier by Use of Ultrasound and Microbubbles: Safety and Efficacy Evaluation in Rhesus Macaques. *Cancer Res.* **72**, 3652–3663 (2012).
35. Downs, M. E. et al. Long-Term Safety of Repeated Blood-Brain Barrier Opening via Focused Ultrasound with Microbubbles in Non-Human Primates Performing a Cognitive Task. *PLOS ONE*. **10**, e0125911 (2015).
36. Pouliopoulos, A. N. et al. A Clinical System for Non-invasive Blood–Brain Barrier Opening Using a Neuronavigation-Guided Single-Element Focused Ultrasound Transducer. *Ultrasound Med. Biol.* **46**, 73–89 (2020).

37. Morse, S. V. et al. Neuron labeling with rhodamine-conjugated Gd-based MRI contrast agents delivered to the brain via focused ultrasound. *Theranostics* **10**, 2659–2674 (2020).
38. Chen, X., Liu, C., Muok, L., Zeng, C. & Li, Y. Dynamic 3D On-Chip BBB Model Design, Development, and Applications in Neurological Diseases. *Cells* **10**, 3183 (2021).
39. Pouliopoulos, A. N. et al. Safety evaluation of a clinical focused ultrasound system for neuronavigation guided blood-brain barrier opening in non-human primates. *Sci. Rep.* **11**, 15043 (2021).
40. Davies, H. J. et al. Imaging With Therapeutic Acoustic Wavelets–Short Pulses Enable Acoustic Localization When Time of Arrival is Combined With Delay and Sum. *IEEE Trans. Ultrason. Ferroelectr. Freq. Control*. **68**, 178–190 (2021).
41. Morse, S. V., Mishra, A., Chan, T. G., De Rosales, T. M., Choi, J. J. & R. & Liposome delivery to the brain with rapid short-pulses of focused ultrasound and microbubbles. *J. Controlled Release*. **341**, 605–615 (2022).
42. Lim, K. et al. Rapid short-pulses of focused ultrasound and microbubbles deliver a range of agent sizes to the brain. *Sci. Rep.* **13**, 6963 (2023).
43. Morse, S. V. et al. Biological effects of rapid short pulses of focused ultrasound for drug delivery to the brain. *J. Control Release Off J. Control Release Soc.* **382**, 113646 (2025).
44. Pereira, M. A., Drevenakova, V., Liu, Q. E., Grewal, S. & Morse, S. V. Enhancing Anti-CTLA-4 Antibody Delivery to the Brain Using Focused Ultrasound and Microbubbles. *ImmunoTargets Ther.* **15**, 1–12 (2026).
45. Gateau, J., Aubry, J. F., Pernot, M., Fink, M. & Tanter, M. Combined passive detection and ultrafast active imaging of cavitation events induced by short pulses of high-intensity ultrasound. *IEEE Trans. Ultrason. Ferroelectr. Freq. Control*. **58**, 517–532 (2011).
46. Andoh, M. & Koyama, R. Comparative Review of Microglia and Monocytes in CNS Phagocytosis. *Cells* **10**, 2555 (2021).
47. Jordão, J. F. et al. Amyloid-β plaque reduction, endogenous antibody delivery and glial activation by brain-targeted, transcranial focused ultrasound. *Exp. Neurol.* **248**, 16–29 (2013).
48. Leinenga, G. & Götz, J. Scanning ultrasound removes amyloid-β and restores memory in an Alzheimer's disease mouse model. *Sci Transl Med* **7**, (2015).
49. Burgess, A. & Hynynen, K. Noninvasive and Targeted Drug Delivery to the Brain Using Focused Ultrasound. *ACS Chem. Neurosci.* **4**, 519–526 (2013).
50. Dittadi, R. et al. Comparison between western blotting, immunohistochemical and ELISA assay for p185neu quantitation in breast cancer specimens. *Anticancer Res.* **13**, 1821–1824 (1993).
51. Shankar, G. M. et al. Biochemical and immunohistochemical analysis of an Alzheimer's disease mouse model reveals the presence of multiple cerebral Aβ assembly forms throughout life. *Neurobiol. Dis.* **36**, 293–302 (2009).

52. Doody, R. S. et al. A Phase 3 Trial of Semagacestat for Treatment of Alzheimer's Disease. *N Engl. J. Med.* **369**, 341–350 (2013).
53. Egan, M. F. et al. Randomized Trial of Verubecestat for Mild-to-Moderate Alzheimer's Disease. *N Engl. J. Med.* **378**, 1691–1703 (2018).
54. Van Dyck, C. H. et al. Lecanemab in Early Alzheimer's Disease. *N Engl. J. Med.* **388**, 9–21 (2023).
55. Salloway, S. et al. Amyloid-Related Imaging Abnormalities in 2 Phase 3 Studies Evaluating Aducanumab in Patients With Early Alzheimer Disease. *JAMA Neurol.* **79**, 13 (2022).
56. Bobola, M. S. et al. Transcranial focused ultrasound, pulsed at 40 Hz, activates microglia acutely and reduces Aβ load chronically, as demonstrated in vivo. *Brain Stimulat*. **13**, 1014–1023 (2020).
57. Grewal, S. et al. Using focused ultrasound to modulate microglial structure and function. *Front. Cell. Neurosci.* **17**, 1290628 (2023).
58. Poon, C. T. et al. Time course of focused ultrasound effects on β-amyloid plaque pathology in the TgCRND8 mouse model of Alzheimer's disease. *Sci. Rep.* **8**, 14061 (2018).
59. Wang, F. et al. Ultrasound Combined With Microbubbles Loading BDNF Retrovirus to Open Blood–Brain Barrier for Treatment of Alzheimer's Disease. *Front. Pharmacol.* **12**, 615104 (2021).
60. Burgess, M. T., Apostolakis, I. & Konofagou, E. E. Power cavitation-guided blood-brain barrier opening with focused ultrasound and microbubbles. *Phys. Med. Biol.* **63**, 065009 (2018).

Figures

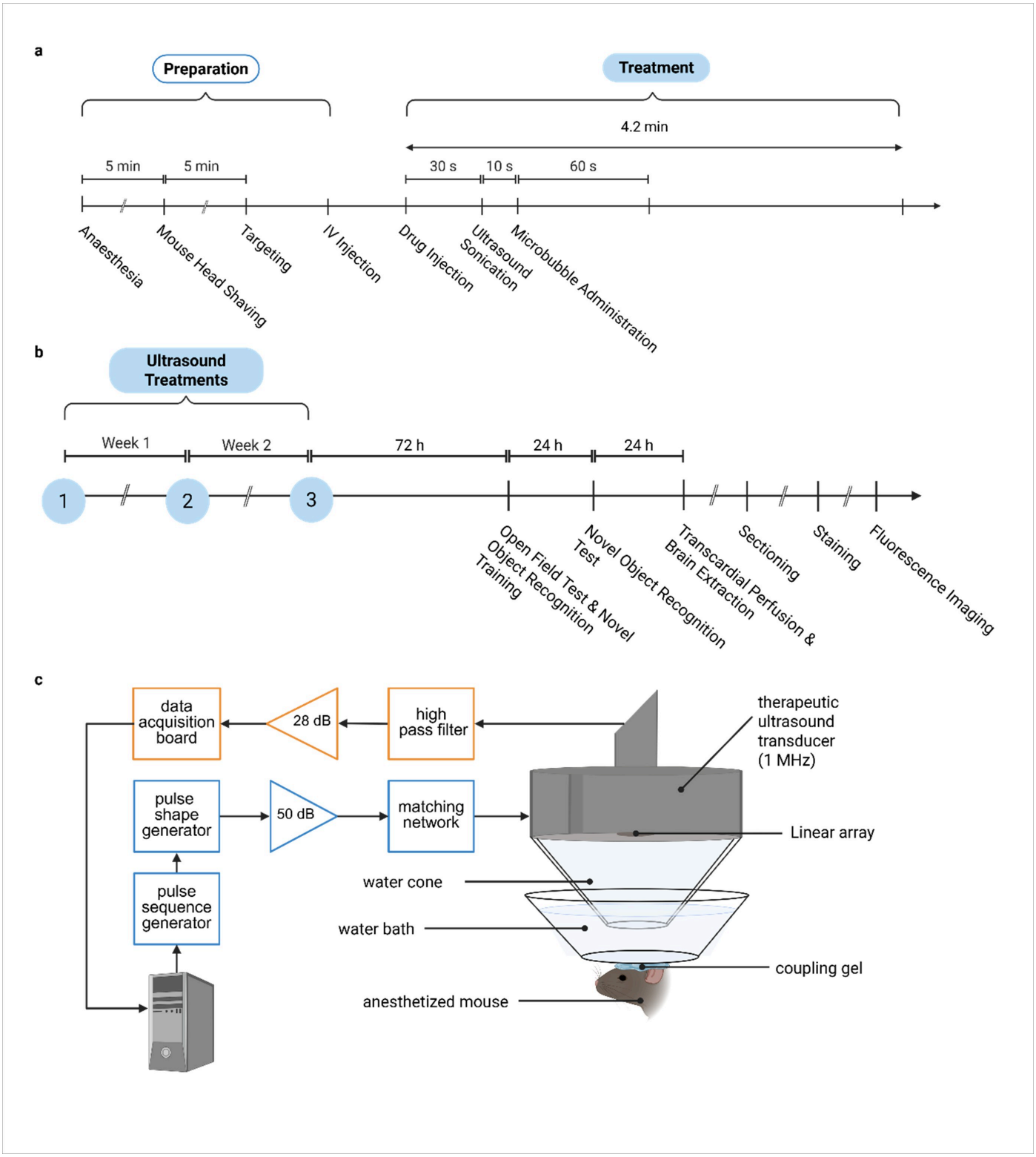


Figure 1

Ultrasound experimental setup and treatment regimen. (a) Timeline of each ultrasound experiment: mice were anaesthetized, head was shaved, and the left hippocampus targeted with ultrasound. The cobalt-based drug was injected intravenously followed by microbubbles before the left hippocampus was exposed to focused ultrasound. **(b)** Timeline of entire chronic treatment: three weekly treatments were followed by open field testing and novel object recognition training 72 hours after the last

treatment, with novel object recognition testing 24 hours after that. Mice were subsequently sacrificed, transcardially perfused and the brain extracted. 5 days after the last ultrasound treatment, brains were sectioned, stained and imaged. **(c)** Experimental setup: rapid short-pulses (RaSP) of ultrasound were emitted (center frequency = 1 MHz, peak-negative pressure = 0.35 MPa, pulse length = 5 cycles, pulse repetition frequency = 1.25 kHz, burst length = 10 ms, burst repetition frequency = 0.5 Hz). An L7-4 linear array co-axially aligned through the center of the therapeutic transducer was used to capture the acoustic emissions from the microbubbles.

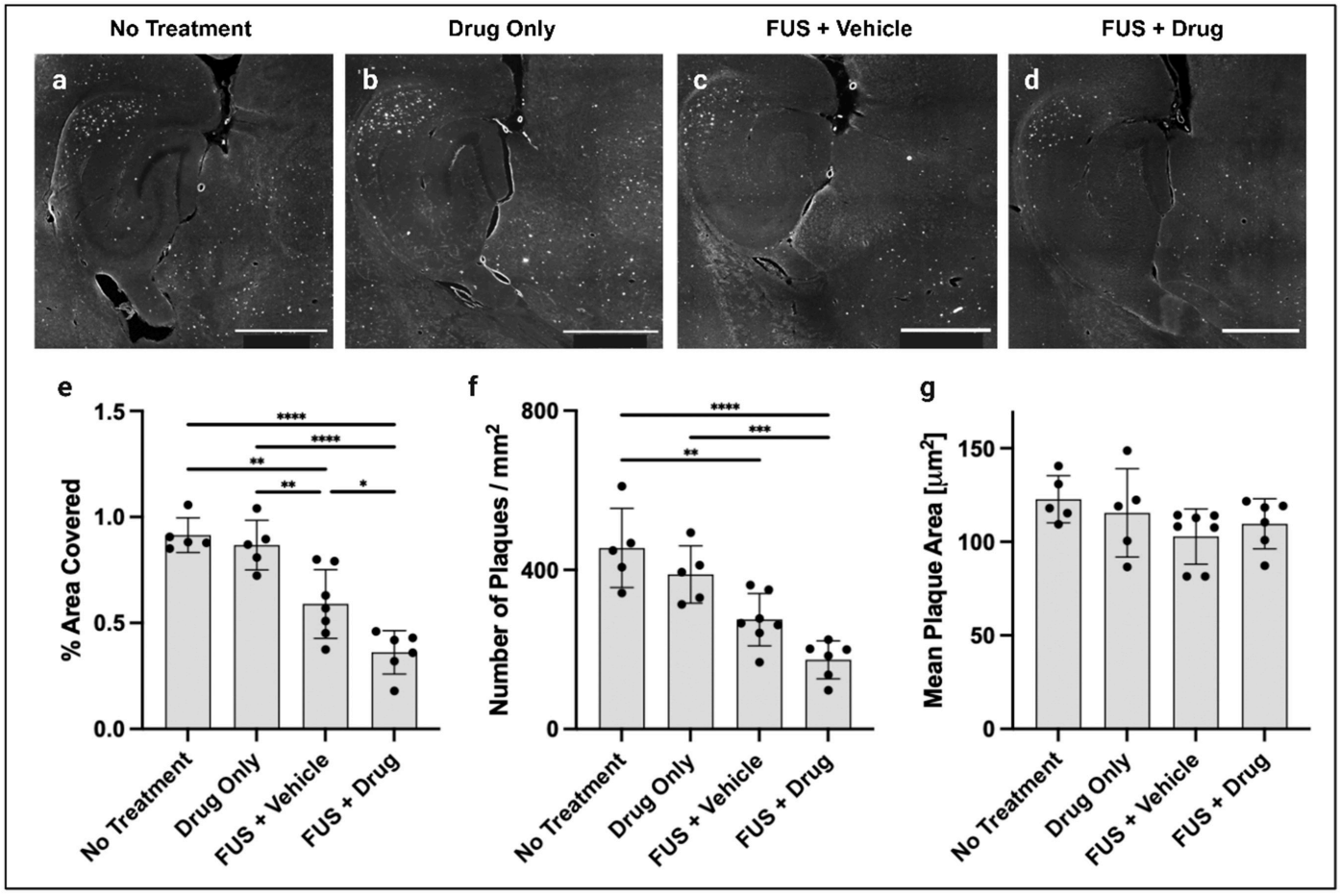


Figure 2

Delivery of the CoLAm2 cobalt-based drug across the blood-brain barrier with focused ultrasound results in a reduction in protein aggregates in 5xFAD mice. Representative fluorescence microscopy

images (**a-d**) of protein aggregates (white) detected by Thio-S staining of brain slices from 5xFAD mice in no-treatment (**a**), drug-only (**b**), FUS + Vehicle (**c**), or FUS + Drug (**d**) groups. Quantification of the left hippocampus and thalamus area of Thio-S-stained images highlight reductions in the percentage of area covered by detectable Thio-S-stained plaques (**e**) and the number of plaques per mm^2 (**f**) in FUS + Vehicle and FUS + Drug treated animals compared to no-treatment and drug-only controls groups. No significant differences ($P > 0.05$) were observed in the mean area occupied by plaques (**g**) between treatment groups. Columns represent mean±SD and statistical analysis included One-way ANOVA with Tukey's multiple comparison post-test, *$P < 0.05$; **$P < 0.01$; ***$P < 0.001$; ****$P < 0.0001$. Scale bars represent 1000 µm.

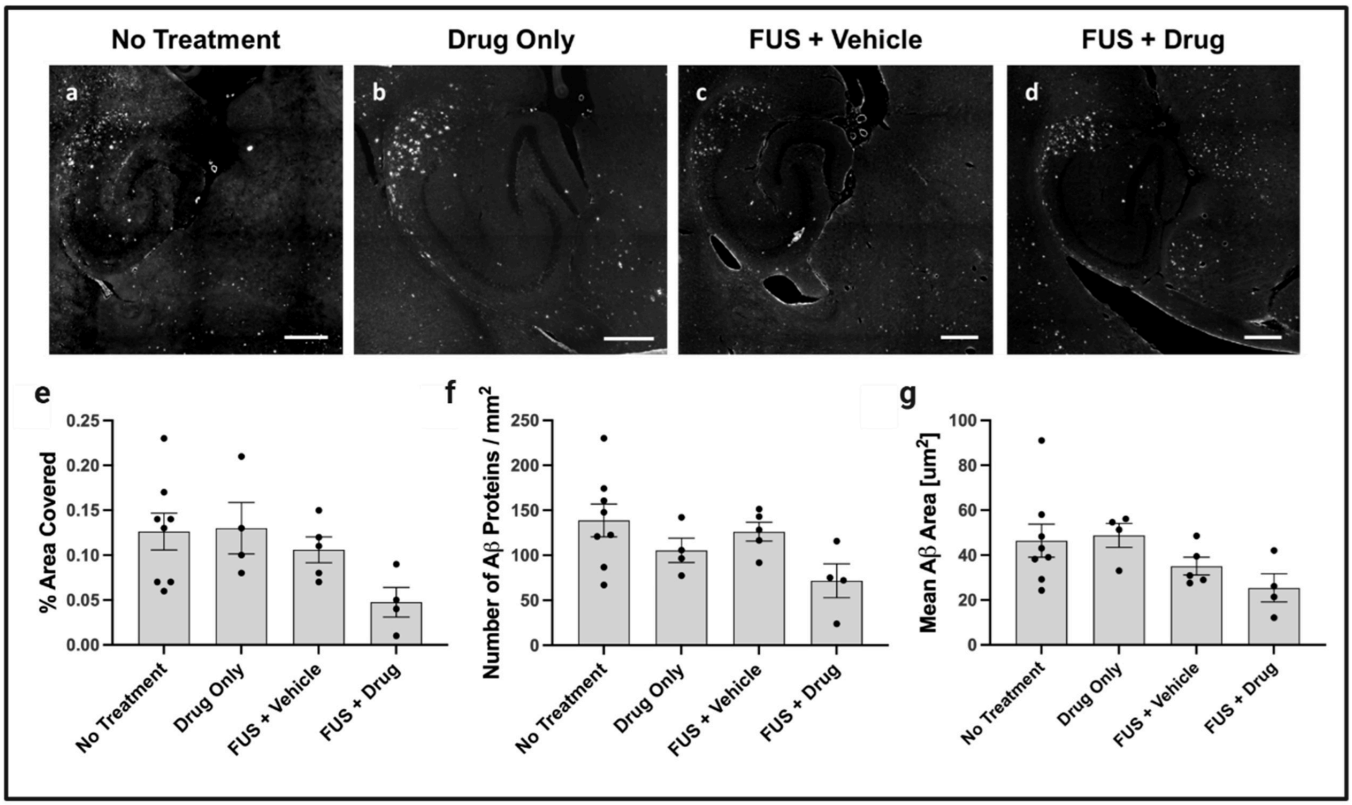


Figure 3

No significant changes in **Amyloid-β load detected in the hippocampus of 5xFAD mice treated with CoLAm2 drug delivered across the blood-brain barrier with focused ultrasound.** Representative

fluorescence microscopy images of MOAB-2-stained brain slices from 5xFAD mice with no treatment (**a**), drug only (**b**), FUS + Vehicle (**c**), or FUS + Drug (**d**) treatment. MOAB-2 staining detects Aβ proteins, including monomers, oligomers and aggregates. Quantification of MOAB-2 staining highlights no significant differences ($P > 0.05$) in the percentage of area covered by detected MOAB-2-stained amyloid beta proteins (**e**), the number of Aβ proteins per mm^2 (**f**), and the mean protein area (**g**) between all treatment groups. Columns represent mean±SD and statistical analysis included One-way ANOVA with Tukey's multiple comparison post-test. Scale bar represents 500 μm.

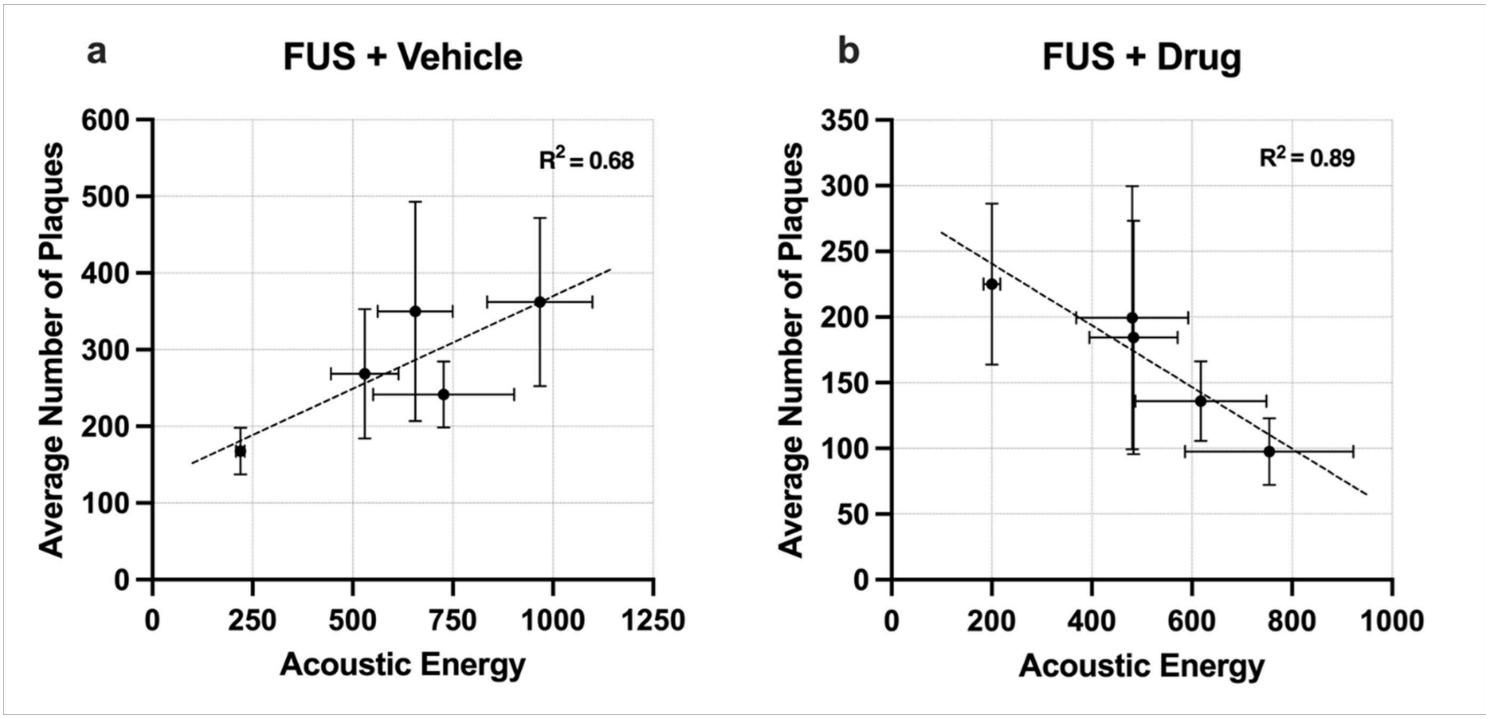


Figure 4

Correlation between the average number of plaques detected and the acoustic energy received from the microbubble emissions during focused ultrasound treatments. The average number of plaques increases with higher acoustic energy detected from microbubble emissions ($R^2 = 0.88$) in mice treated with FUS + Vehicle (**a**), whilst the average number of plaques decreases with increasing acoustic energy ($R^2 = 0.68$) in FUS + Drug treated mice (**b**). Microbubble emissions were captured using Passive Acoustic Mapping (PAM). Each data point represents one mouse.

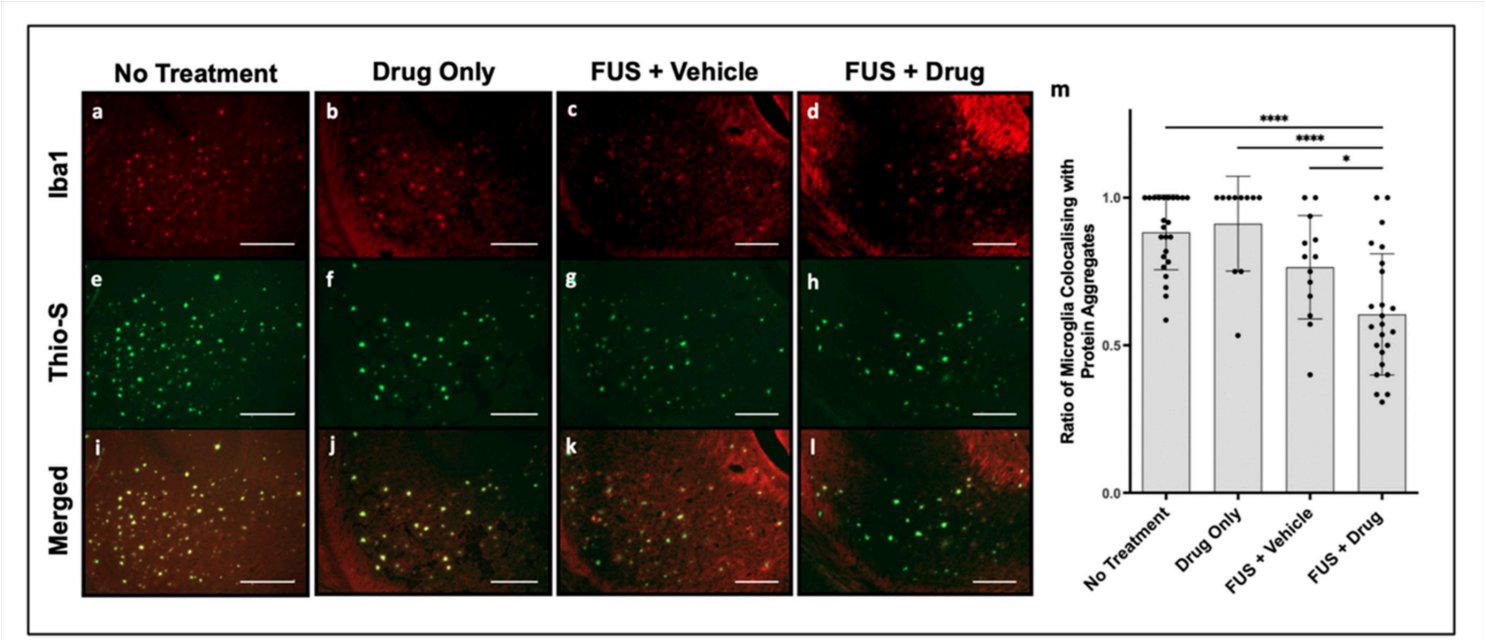


Figure 5

Reduction in the number of microglia surrounding protein aggregates in 5xFAD mice with cobalt-based CoLAm2 drug delivery via focused ultrasound. Representative fluorescence microscopy images of Iba1-positive microglia (**a-d**) co-stained with Thio-S (**e-h**), and merged channels (**i-l**) for no-treatment (**a, e, i**), drug-only (**b, f, j**), FUS + Vehicle (**c, g, k**), and FUS + Drug (**d, h, l**) treatment groups. Quantification of the ratio of microglia colocalizing with Thio-S-stained protein aggregates highlights a significant reduction between no-treatment, drug-only, and FUS + Vehicle groups and FUS + Drug-treated mice (**m**). Columns represent mean±SD and statistical analysis included One-way ANOVA with Tukey's multiple comparison post-test, *P < 0.05; ****P<0.0001. Scale bars represent 200 μm.

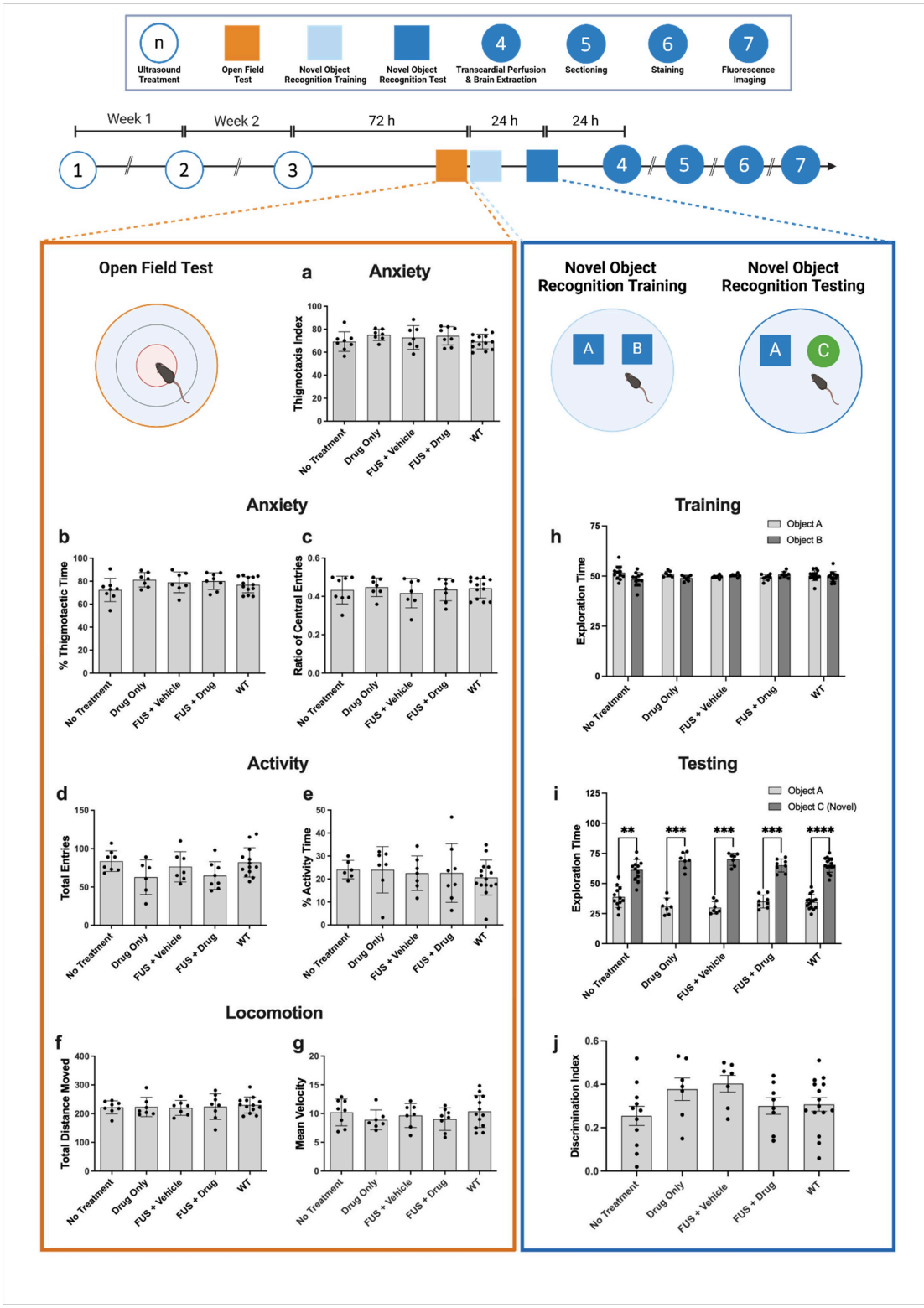


Figure 6

No significant differences in behavior between treatment groups. Experimental timeline of ultrasound treatments followed by behavioral testing (open field and novel object recognition) and post-processing of the brains (**top**). Quantification of the data obtained from the open field testing (**a-g**) shows no significant differences ($P > 0.05$) in the behavior of 5xFAD mice of all treatment groups and healthy wild-type (WT) mice in terms of measurements related to anxiety (**a-c**), activity (**d-e**), and locomotion (**f-g**).

Novel object recognition testing results (**h-j**) showcase an expected similar exploration time between identical Object A and B during training (**h**), and significant differences between Object A and Novel Object C during testing (**i**, $P < 0.05$). No significant differences are seen in the discrimination index between treatment groups (**j**, $P > 0.05$). These results show that all treatments are not negatively affecting the behaviour of these mice. Columns represent mean±SD, **P < 0.01; ***P < 0.001; ****P < 0.0001.

Supplementary Files

This is a list of supplementary files associated with this preprint. Click to download.

- Supplementaryinformation.pdf
- Supplementaryinformation.docx